

ISOTHERMAL BONDI ACCRETION IN JAFFE AND HERNQUIST GALAXIES WITH A CENTRAL BLACK HOLE: FULLY ANALYTICAL SOLUTIONS

LUCA CIOTTI* AND SILVIA PELLEGRINI

Department of Physics and Astronomy, University of Bologna, via Piero Gobetti 93/2, 40129 Bologna, Italy

*E-mail: luca.ciotti@unibo.it

ABSTRACT

One of the most active fields of research of modern-day astrophysics is that of massive black hole formation and co-evolution with the host galaxy. In these investigations, ranging from cosmological simulations, to semi-analytical modeling, to observational studies, the Bondi solution for accretion on a central point mass is widely adopted. In this work we generalize the classical Bondi accretion theory to take into account the effects of the gravitational potential of the host galaxy, and of radiation pressure in the optically thin limit. Then, we present the fully analytical solution, in terms of the Lambert-Euler W -function, for isothermal accretion in Jaffe and Hernquist galaxies with a central black hole. The flow structure is found to be sensitive to the shape of the mass profile of the host galaxy. These results and the formulae that are provided, mostly important the one for the critical accretion parameter, allow for a direct evaluation of all flow properties, and are then useful for the above mentioned studies. As an application, we examine the departure from the true mass accretion rate of estimates obtained using the gas properties at various distances from the black hole, under the hypothesis of classical Bondi accretion. An overestimate is obtained from regions close to the black hole, and an underestimate outside a few Bondi radii; the exact position of the transition between the two kinds of departure depends on the galaxy model.

Keywords: galaxies: elliptical and lenticular, cD – accretion: spherical accretion – X-rays: galaxies – X-rays: ISM

1. INTRODUCTION

Bondi (1952) presented the solution for spherically-symmetric, steady accretion of a spatially infinite gas distribution on to an isolated central point mass. This solution in the recent years became a standard and intensively adopted tool for estimates of the scale-radius and the mass flow rate in studies of accretion on massive black holes (hereafter MBH) at the center of galaxies. In fact, the discovery of the ubiquitous presence of MBHs at the center of spheroids on one side (Kormendy & Richstone 1995), and the enormous advance in instrumental capabilities, computer performances and numerical astrophysics on the other, triggered a huge increase in the number of investigations involving the accretion phenomenon at the center of galaxies. These studies range from observational works deriving the gas properties in regions surrounding the MBHs (see, e.g., Baganoff et al. 2003; Pellegrini 2005, 2010; Rafferty et al. 2006; Kormendy & Ho 2013; Wong et al. 2014; Russell et al. 2015), to theoretical studies on the origin of the various types of AGN sources, and on the various physical processes involved in accretion on to a MBH (e.g., Bu et al. 2013, Yuan & Narayan 2014, Cao 2016, Park et al. 2017), to cosmological investigations of MBH formation, and co-evolution of MBHs and host galaxies involving the “feedback” action (see, e.g., Sijacki et al. 2007; Hopkins et al. 2006, 2007; Di Matteo et al. 2008; Park & Ricotti 2011; Volonteri et al. 2015; Choi et al. 2016; DeGraf et al. 2017). Unfortunately, in general these studies lack the resolution to follow gas transport down to the parsec scale, and the Bondi model is used as the starting point for estimates of the accretion radius (i.e., the sonic radius), and of the mass accretion rate. In particular, the Bondi accretion rate gives the mass supply to the MBH by taking the density and temperature at some finite distance from the center, implicitly assuming that these values represent the true boundary conditions (i.e., at infinity) for the Bondi problem. Even the knowledge of the true boundary conditions, though, would not be enough for a proper treatment of the real problem, because the MBH is not an isolated point-mass, but resides at the bottom of the potential well of the host galaxy. Moreover, the radiation emitted by the inflowing material may interact with it, accretion may become unsteady, and Bondi accretion during phases of AGN feedback cannot be applied (e.g., Ciotti

& Ostriker 2012). During phases of moderate accretion (in the “maintainance” mode), instead, when the problem can be considered almost steady, Bondi accretion could provide a reliable approximation of the real situation.

In Korol et al. (2016, hereafter KCP16), we generalized the Bondi problem to mass accretion at the center of galaxies, including also the effect of electron scattering on the accreting gas. We then calculated the deviation from the true values of estimates of the Bondi radius and mass accretion rate due to adopting as boundary values for the density and temperature those at a finite distance from the MBH, and assuming the validity of the classical Bondi accretion solution. In the case of the Hernquist galaxy model, we showed how to obtain the analytical expression for the critical value of the accretion parameter λ_{cr} , for generic values of the polytropic index γ . However, even for this exceptional case, the radial profiles of the properties of the accreting gas remained to be determined numerically. Of course, in observational studies, or in numerical simulations where subgrid MBH accretion is implemented, analytical solutions for these radial profiles would be very useful. Here we show that, remarkably, the whole accretion problem can be solved in a *fully* analytical way for the *isothermal* accretion in Jaffe (1993) and Hernquist galaxy models with central MBHs. This is due to the fact that 1) for these two models it is possible to obtain explicitly λ_{cr} , and 2) in isothermal accretion in generic spherically symmetric potentials the radial profile of the Mach number can be explicitly written in terms of the *Lambert-Euler W*-function. The possibility of using the *W*-function to describe isothermal flows had been pointed out when discussing the isothermal Parker solution for the solar wind [Cranmer 2004; see also Herbst (2015) for the case of accretion]. At the best of our knowledge, the present work provides the first fully analytical solution of the accretion problem on a MBH at the center of a galaxy.

This paper is organized as follows. In Section 2 we recall the main properties of the classical Bondi solution, and we present the fully analytical isothermal solution for accretion onto an isolated MBH. In Section 3 we consider the generalized case of the Bondi solution in presence of radiation feedback and of a galaxy potential hosting the central MBH. Section 4 deals with the Jaffe and Hernquist galaxy models, and presents the fully analytical solution for them. In Section 5 we examine the departure of the estimate of the mass accretion rate from the true value, when the estimate is obtained using as boundary values for the density and temperature those at points along the solution at finite distance from the MBH. The main conclusions are summarized in Section 6, and technical details are given in the Appendixes.

2. THE CLASSICAL BONDI MODEL

We shortly recall here the main properties of the classical, polytropic Bondi accretion model, even though the present investigation focusses on isothermal accretion. The gas is perfect, has a spatially infinite distribution, and is accreting on to an isolated central mass, in our case a MBH, of mass M_{BH} . The gas density and pressure are linked by:

$$p = \frac{k_{\text{B}}\rho T}{\mu m_{\text{p}}} = p_{\infty}\tilde{\rho}^{\gamma}, \quad \tilde{\rho} \equiv \frac{\rho}{\rho_{\infty}}, \quad (1)$$

where $1 \leq \gamma \leq 5/3$ is the polytropic index, m_{p} is the proton mass, μ is the mean molecular weight, k_{B} is the Boltzmann constant, and p_{∞} and ρ_{∞} are respectively the gas pressure and density at infinity. The polytropic gas sound speed is

$$c_{\text{s}}^2 = \gamma \frac{p}{\rho}. \quad (2)$$

The isothermal case is recovered for $\gamma = 1$. The time-independent continuity equation is:

$$4\pi r^2 \rho(r) v(r) = \dot{M}_{\text{B}}, \quad (3)$$

where $v(r)$ is the gas radial velocity, and \dot{M}_{B} is the time-independent accretion rate on the MBH. The Bernoulli equation, with the appropriate boundary conditions at infinity, becomes:

$$\frac{v(r)^2}{2} + \Delta h(r) - \frac{GM_{\text{BH}}}{r} = 0, \quad (4)$$

where, from eq. (1)

$$\Delta h \equiv \int_{p_{\infty}}^p \frac{dp}{\rho} = c_{\infty}^2 \times \begin{cases} \frac{\tilde{\rho}^{\gamma-1} - 1}{\gamma - 1}, & \gamma > 1, \\ \ln \tilde{\rho}, & \gamma = 1, \end{cases} \quad (5)$$

and c_{∞} is the sound speed of the gas at infinity.

An important scalelength of the problem, the so-called Bondi radius, is naturally defined as

$$r_B \equiv \frac{GM_{\text{BH}}}{c_\infty^2}. \quad (6)$$

In the following we will use r_B as given by the definition above as the length scale, even when considering more general models. After introducing the normalized quantities

$$x \equiv \frac{r}{r_B}, \quad \tilde{c}_s \equiv \frac{c_s}{c_\infty} = \tilde{\rho}^{\frac{\gamma-1}{2}}, \quad \mathcal{M} = \frac{v}{c_s}, \quad (7)$$

where \mathcal{M} is the Mach number, eqs. (3)-(4) become respectively

$$x^2 \mathcal{M} \tilde{\rho}^{\frac{\gamma+1}{2}} = \frac{\dot{M}_B}{4\pi r_B^2 \rho_\infty c_\infty} \equiv \lambda, \quad (8)$$

$$\begin{cases} \frac{\mathcal{M}^2 \tilde{c}_s^2}{2} + \frac{\tilde{\rho}^{\gamma-1}}{\gamma-1} = \frac{1}{x} + \frac{1}{\gamma-1}, & \gamma > 1, \\ \frac{\mathcal{M}^2 \tilde{c}_s^2}{2} + \ln \tilde{\rho} = \frac{1}{x}, & \gamma = 1. \end{cases} \quad (9)$$

λ is the dimensionless accretion parameter, that determines the accretion rate for assigned M_{BH} and boundary conditions. From eqs. (7)-(8), the radial profile of all hydrodynamical properties can be expressed in terms of $\mathcal{M}(x)$. By elimination of $\tilde{\rho}$ in eqs. (8)-(9), for $1 < \gamma \leq 5/3$ the Bondi problem reduces to the solution of the equation

$$g(\mathcal{M}) = \Lambda f(x), \quad \Lambda \equiv \lambda^{\frac{2(1-\gamma)}{\gamma+1}}, \quad (10)$$

where

$$g(\mathcal{M}) \equiv \mathcal{M}^{\frac{2(1-\gamma)}{\gamma+1}} \left(\frac{\mathcal{M}^2}{2} + \frac{1}{\gamma-1} \right), \quad (11)$$

and

$$f(x) \equiv x^{\frac{4(\gamma-1)}{\gamma+1}} \left(\frac{1}{x} + \frac{1}{\gamma-1} \right). \quad (12)$$

As well known, Λ cannot be chosen arbitrarily; in fact, both $g(\mathcal{M})$ and $f(x)$ have a minimum:

$$g_{\min} = \frac{\gamma+1}{2(\gamma-1)}, \quad \text{for } \mathcal{M}_{\min} = 1, \quad (13)$$

and

$$f_{\min} = \frac{\gamma+1}{4(\gamma-1)} \left(\frac{4}{5-3\gamma} \right)^{\frac{5-3\gamma}{\gamma+1}}, \quad \text{for } x_{\min} = \frac{5-3\gamma}{4}. \quad (14)$$

Therefore, to satisfy eq. (10) $\forall x > 0$ requires that $g_{\min} \leq \Lambda f_{\min}$, i.e., that $\Lambda \geq \Lambda_{\text{cr}} \equiv g_{\min}/f_{\min}$. In order for the solution to exist it is then required that:

$$\lambda \leq \lambda_{\text{cr}} = \left(\frac{f_{\min}}{g_{\min}} \right)^{\frac{\gamma+1}{2(\gamma-1)}} = \frac{1}{4} \left(\frac{2}{5-3\gamma} \right)^{\frac{5-3\gamma}{2(\gamma-1)}}. \quad (15)$$

In particular $\lambda_{\text{cr}} = e^{3/2}/4$ for $\gamma \rightarrow 1^+$, and $\lambda_{\text{cr}} = 1/4$ for $\gamma \rightarrow 5/3^-$.

In the isothermal case the Bondi problem is given by:

$$\begin{cases} g(\mathcal{M}) = f(x) - \Lambda, & \Lambda \equiv \ln \lambda, \\ g(\mathcal{M}) \equiv \frac{\mathcal{M}^2}{2} - \ln \mathcal{M}, \\ f(x) \equiv \frac{1}{x} + 2 \ln x, \end{cases} \quad (16)$$

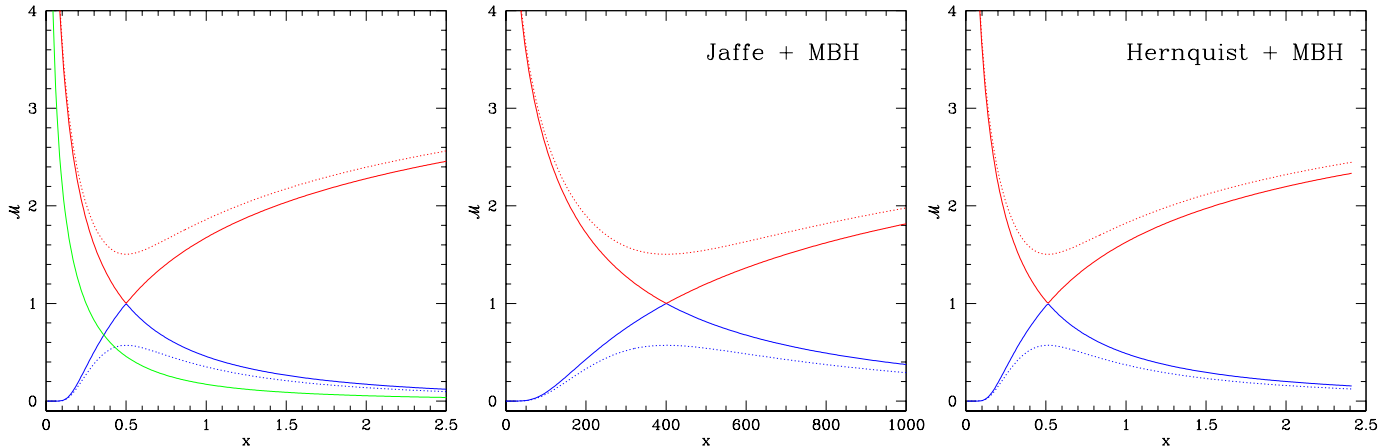


Figure 1. Mach number profile $\mathcal{M}(x)$ for isothermal Bondi accretion on a MBH. Blue lines show the subsonic regime, red lines the supersonic one. The leftmost panel refers to classical Bondi accretion (Sect. 2.1), and the green line refers to the inclusion of the effect of radiation pressure for $\chi = 0.5$ (Sect. 3.1). The middle and right panels show respectively accretion at the center of a Jaffe and an Hernquist galaxy model, with $\mathcal{R} = 1000$, $\xi = 100$ and $\chi = 1$ (Sects. 4.1 and 4.2). Solid lines show the two critical solutions, one in which \mathcal{M} continuously increases towards the center, and the other in which the flow starts supersonic and reaches the center with zero velocity. The dotted lines show the illustrative example of the two subcritical solutions with $\lambda = 0.8\lambda_{\text{cr}}$. Note how, for this particular choice of the \mathcal{R} and ξ values, the position of the sonic point moves considerably outward in presence of a Jaffe galaxy (Sect. 4.1); for the Hernquist one, instead, the sonic point is similar to that of the classical Bondi accretion, that is it remains small (Sect. 4.2).

with

$$\begin{cases} g_{\min} = \frac{1}{2}, & \text{for } \mathcal{M}_{\min} = 1, \\ f_{\min} = 2 - 2 \ln 2, & \text{for } x_{\min} = \frac{1}{2}, \end{cases} \quad (17)$$

so that solutions exist only for $g_{\min} \leq f_{\min} - \Lambda$, i.e., for $\Lambda \leq \Lambda_{\text{cr}} \equiv f_{\min} - g_{\min}$. Equation (17) then requires

$$\lambda \leq \lambda_{\text{cr}} = e^{f_{\min} - g_{\min}} = \frac{e^{3/2}}{4}, \quad (18)$$

in accordance with the limit of eq. (15) for $\gamma \rightarrow 1^+$. In the following, the function $f(x)$ in eq. (16) is generalized by considering the effect of radiation pressure due to electron scattering, and the additional gravitational field of the host galaxy.

Summarizing, the solution of the Bondi problem requires to obtain the radial profile $\mathcal{M}(x)$, for given $\lambda \leq \lambda_{\text{cr}}$ (see, e.g., Bondi 1952; Frank, King & Raine 1992). Unfortunately, eq. (10) does not have an explicit solution in terms of known functions for generic values of γ , and must be solved numerically.

2.1. The isothermal solution

Among the two critical solutions characterizing the Bondi problem, we consider that pertinent to accretion, with an increasing Mach number approaching the center. Appendix A shows how introducing the Lambert-Euler function W , and using eq. (A3) with $a = 1/2$, $b = 2$, $c = 0$, $d = -1$, $X = \mathcal{M}$ and $Y = f(x) - \Lambda$, one can solve eq. (16) for $\mathcal{M}(x)$, and then recover the full solution for isothermal accretion. In particular, along the critical solution, when $\lambda = \lambda_{\text{cr}}$, \mathcal{M}^2 is given by:

$$\mathcal{M}^2 = - \begin{cases} W \left(0, -\frac{e^{3-2/x}}{16x^4} \right), & x \geq x_{\min}, \\ W \left(-1, -\frac{e^{3-2/x}}{16x^4} \right), & 0 < x \leq x_{\min}, \end{cases} \quad (19)$$

where $x_{\min} = 1/2$ [eq. (17)].

The properties of the critical solution (19) can be visualized with the help of Fig. 5 in Appendix A. Figure 5 shows that only for a negative argument W assumes negative values, and so \mathcal{M}^2 can be a positive quantity. As x decreases from infinity to the sonic point $x_{\min} = 1/2$, the argument z of the $W(0, z)$ function decreases from 0 to $-1/e$, and the function $W(0, z)$ decreases from 0 to -1 , i.e. from point A to point B (solid line in Fig. 5). Then, when x decreases further approaching the origin, the argument of the branch $W(-1, z)$ increases again from $-1/e$ to 0, and W decreases from -1 to $-\infty$, moving from point B to the asymptotic point C (dashed line in Fig. 5). Note that the $W(-1, z)$ function describes supersonic accretion, while $W(0, z)$ subsonic accretion, so that the critical solution is obtained by connecting together the two branches. This is illustrated by the red and blue solid lines, respectively, in Fig. 1. Note also that, in case of isothermal accretion with $\lambda < \lambda_{\text{cr}}$, the continuous solutions are limited to a subset of the regions A - B (the subsonic accretion branch, blue dotted lines), or to a subset of the region B - C (the supersonic accretion branch, red dotted lines).

Having obtained $\mathcal{M}(x)$, from eq. (8) with $\gamma = 1$ one has:

$$\tilde{\rho}(x) = \frac{\lambda_{\text{cr}}}{x^2 \mathcal{M}(x)}, \quad (20)$$

while the modulus of the accretion velocity is $v(r) = c_{\infty} \mathcal{M}(x)$.

3. GENERALIZED BONDI ACCRETION FOR AN ISOTHERMAL FLOW

3.1. Adding the effect of electron scattering

The Bondi solution describes a purely hydrodynamical flow, where heat exchanges are implicitly taken into account by the polytropic index¹ (see also KCP16, Sect. 3). In real cases the flow can be affected by the emission of radiation near the MBH; in terms of the mass accretion rate \dot{M}_{acc} , this is expressed by

$$L = \varepsilon \dot{M}_{\text{acc}} c^2, \quad (21)$$

where ε is the radiative efficiency. For example, in the classical Bondi accretion one would adopt $\dot{M}_{\text{acc}} = \dot{M}_{\text{B}}$. The efficiency ε can depend on \dot{M}_{acc} , as in the advection dominated accretion at low \dot{M}_{acc} (e.g., Yuan & Narayan 2014), when ε is very low. At high accretion rates, instead, the efficiency is $\varepsilon_0 \simeq 0.1$, and the effects of the emitted radiation can be sufficiently strong to stop accretion; in these circumstances, the steady Bondi solution cannot be applied, even approximately (e.g., Ciotti & Ostriker 2012 for a review).

KCP16 extended the classical Bondi accretion solution by including the radiation pressure effect due to electron scattering in the optically thin regime (see also Fukue 2001; Lusso & Ciotti 2011). Under the assumption of spherical symmetry, the total (gravity plus radiation) force on a gas element is:

$$F(r) = -\frac{GM_{\text{BH}}\rho(r)\chi}{r^2}, \quad \chi \equiv 1 - l, \quad l \equiv \frac{L}{L_{\text{Edd}}}, \quad (22)$$

where $L_{\text{Edd}} = 4\pi cGM_{\text{BH}}m_{\text{p}}/\sigma_{\text{T}}$ is the Eddington luminosity, and $\sigma_{\text{T}} = 6.65 \times 10^{-25} \text{cm}^2$ is the Thomson cross section. When $L = L_{\text{Edd}}$, and then $\chi = 0$, radiation pressure cancels exactly the MBH gravitational field at all radii; when $\chi = 1$, the radiation pressure has no effect on the accretion flow. We define \dot{M}_{es} as the accretion rate under the above hypotheses; then, in terms of the Eddington mass accretion rate \dot{M}_{Edd} , one has:

$$\dot{M}_{\text{Edd}} \equiv \frac{L_{\text{Edd}}}{\varepsilon_0 c^2}, \quad l = \frac{\dot{M}_{\text{es}}}{\dot{M}_{\text{Edd}}} \frac{\varepsilon}{\varepsilon_0}. \quad (23)$$

As demonstrated by KCP16, the value of L_{Edd} to be inserted in eqs. (22) and (23) remains that corresponding to the gravity produced only by the MBH, even when the gravitational potential of the host galaxy is also present.

The radiation feedback can be implemented as a correction that reduces the effective gravitational force of the MBH by the factor χ . In particular, for $\gamma = 1$ the function f in eq. (16) becomes:

$$f(x) = \frac{\chi}{x} + 2 \ln x, \quad (24)$$

and the position of the minimum of the new f moves inward with respect to the classical case:

$$x_{\min} = \frac{\chi}{2}. \quad (25)$$

¹ γ is not necessarily the adiabatic index γ_{ad} , so that in the Bondi solution the entropy of the gas can change along the radial streamlines. For a polytropic transformation, of specific heat at constant volume C_V , the molar specific heat is $C = C_V(\gamma_{\text{ad}} - \gamma)/(1 - \gamma)$ (e.g., Chandrasekhar 1939). Therefore $C < 0$ when $1 < \gamma < \gamma_{\text{ad}}$, and the fluid element loses energy as it moves inward and heats.

From the value of x_{\min} and $f_{\min} = f(x_{\min})$, one derives the critical value of the accretion parameter, that we now call λ_{es} :

$$\lambda_{\text{es}} = \chi^2 \lambda_{\text{cr}}, \quad (26)$$

where λ_{cr} is the critical parameter in the corresponding classical case. In turn, the new accretion rate, \dot{M}_{es} , is reduced with respect to \dot{M}_{B} , for given M_{BH} and boundary conditions at infinity:

$$\dot{M}_{\text{es}} = 4\pi r_{\text{B}}^2 \lambda_{\text{es}} \rho_{\infty} c_{\infty} = \frac{\lambda_{\text{es}}}{\lambda_{\text{cr}}} \dot{M}_{\text{B}} = \chi^2 \dot{M}_{\text{B}}. \quad (27)$$

The equation above is actually an implicit equation for \dot{M}_{es} , because χ depends on \dot{M}_{es} itself through eqs. (22)-(23). It can be shown that \dot{M}_{es} self-regulates, and cannot exceed \dot{M}_{Edd} , regardless of the size of \dot{M}_{B} (see KCP16 for a more detailed discussion).

We then use the same procedure of Sect. 2.1 to derive the Mach profile of the critical isothermal solution, for generic values of χ ; $\mathcal{M}(x)$ is now given by:

$$\mathcal{M}^2 = - \begin{cases} W\left(0, -\frac{\chi^4 e^{3-2\chi/x}}{16x^4}\right), & x \geq x_{\min}, \\ W\left(-1, -\frac{\chi^4 e^{3-2\chi/x}}{16x^4}\right), & 0 < x \leq x_{\min}, \end{cases} \quad (28)$$

where now $x_{\min} = \chi/2$. In Fig. 1 (left panel), the green line compares the \mathcal{M} profile of the critical solution with that of the classical Bondi problem, for the illustrative case $\chi = 0.5$; as dictated by eq. (25), the sonic radius moves inward, with $x_{\min} = 1/4$. The density profile, setting $\gamma = 1$ in eq. (8), becomes:

$$\tilde{\rho}(x) = \frac{\lambda_{\text{es}}}{x^2 \mathcal{M}(x)}. \quad (29)$$

3.2. Adding the potential of the galaxy

We now move to the most general problem of Bondi accretion with electron scattering in the potential of the galaxy hosting the MBH at its center. We write the gravitational potential of a spherical galaxy of finite total mass M_{g} as

$$\phi_{\text{g}} = -\frac{GM_{\text{g}}}{r_{\text{g}}} \psi\left(\frac{r}{r_{\text{g}}}\right), \quad (30)$$

where r_{g} and ψ are respectively a characteristic scale-length, and the dimensionless galaxy potential. We assume that $\psi = 0$ for $r \rightarrow \infty$, so that the Bernoulli constant in eq. (4) can still be fixed at infinity. We further introduce the parameters

$$\mathcal{R} \equiv \frac{M_{\text{g}}}{M_{\text{BH}}}, \quad \xi \equiv \frac{r_{\text{g}}}{r_{\text{B}}}, \quad (31)$$

with which the effective total potential becomes:

$$\phi_{\text{t}} = -\frac{GM_{\text{BH}}}{r_{\text{B}}} \left[\frac{\chi}{x} + \frac{\mathcal{R}}{\xi} \psi\left(\frac{x}{\xi}\right) \right]. \quad (32)$$

The function $f(x)$ in eq. (16) is now written as:

$$f = \frac{\chi}{x} + \frac{\mathcal{R}}{\xi} \psi\left(\frac{x}{\xi}\right) + 2 \ln x. \quad (33)$$

Therefore the values of x_{\min} , f_{\min} , and of the critical accretion parameter (that now we call λ_{t}) depend on (χ, \mathcal{R}, ξ) , while the function $g(\mathcal{M})$ is unaffected by the addition of the galaxy potential. Note how, for $\mathcal{R} \rightarrow 0$ (or $\xi \rightarrow \infty$), the galaxy contribution vanishes, $\lambda_{\text{t}} = \lambda_{\text{es}}$, and one recovers the solution of Sect. 3.1. In the limiting case of $\chi = 0$, the problem reduces to Bondi accretion in the potential of the galaxy only, without electron scattering and MBH.

The presence of a galaxy changes the accretion rate, that we now call \dot{M}_{t} ; eq. (8) still holds, with:

$$\dot{M}_{\text{t}} = 4\pi r_{\text{B}}^2 \lambda_{\text{t}} \rho_{\infty} c_{\infty} = \frac{\lambda_{\text{t}}}{\lambda_{\text{cr}}} \dot{M}_{\text{B}}, \quad (34)$$

where again \dot{M}_{B} is the classical Bondi accretion rate for the same chosen boundary conditions ρ_{∞} and c_{∞} .

The radial trend of the Mach number for the critical solution can be derived again along the lines described in Sect. 2.1; we now have:

$$\mathcal{M}^2 = - \begin{cases} W(0, -e^{-2f+2\Lambda_t}), & x \geq x_{\min} \\ W(-1, -e^{-2f+2\Lambda_t}), & 0 < x \leq x_{\min} \end{cases} \quad (35)$$

where $\Lambda_t = \ln \lambda_t = f_{\min} - g_{\min}$ as explained in Sect. 2. Finally, we have

$$\tilde{\rho}(x) = \frac{\lambda_t}{x^2 \mathcal{M}(x)}. \quad (36)$$

The full solution is then known, provided x_{\min} is known. For a generic galaxy model, x_{\min} , f_{\min} , and λ_t can be determined only numerically. Moreover, the galaxy potential can produce more than one minimum for $f(x)$ (KCP16). As we will see in the next Section, two of the most common galaxy models remarkably allow for an analytical expression for x_{\min} and Λ_t , in the isothermal case; therefore, *together with the expression above for \mathcal{M}* , we have a *fully analytical solution of isothermal accretion on MBHs at the center of such galaxies*.

Note that along the critical solution the argument of the exponential in eq. (35) is $-2(f - f_{\min}) - 1$; thus, as x decreases from infinity to x_{\min} , the argument z decreases from 0 to $-1/e$, and the W -function moves from A to $B = (-1/e, -1)$ in Fig. 5 of Appendix A, corresponding to the sonic point. Decreasing x further, the solution switches on the $W(-1, z)$ branch, and the Mach number diverges at the center. For $\Lambda < \Lambda_t$, the subsonic and supersonic cases are again described respectively by the $W(0, z)$ and $W(-1, z)$ branches.

4. TWO FULLY ANALYTICAL CASES: JAFFE AND HERNQUIST GALAXY MODELS WITH A CENTRAL MBH

In this Section we present the final goal of our investigation, the analytical solution for all quantities describing accretion, in the isothermal case, for two particular galaxy models, the Hernquist (1990) and the Jaffe (1983) models with a central MBH. These density profiles describe well the mass distribution of early-type galaxies; they belong to the widely used family of the so-called γ -models (Dehnen 1993, Tremaine et al. 1994), that all have similar $\sim r^{-4}$ density profiles in their external regions (outside r_g). For example, the Hernquist model with a central MBH has been recently adopted for a numerical investigation of bulge-driven, Bondi fueling of seed black holes (Park et al. 2016). As already noticed, λ_t is known once the *absolute* minimum $f_{\min}(\chi, \mathcal{R}, \xi)$ is known; this, in turn, requires the determination of $x_{\min}(\chi, \mathcal{R}, \xi)$. Quite remarkably, for the Hernquist model x_{\min} can be derived analytically in the general polytropic case, solving a cubic equation (KCP16). A peculiar property of such equation is the possibility to present *two* minima for $x > 0$, depending on the galaxy parameters; KCP16 provided the formulae needed to determine the critical points of f , for any choice of γ and of the galaxy parameters, but the final expressions for x_{\min} and f_{\min} were not given. Here we give these analytical expressions for x_{\min} and f_{\min} , in case of isothermal accretion. In addition, we show that λ_t can be evaluated explicitly also for isothermal accretion in the Jaffe model; to our knowledge, these are the only two known cases of fully solvable accretion problems. As we will see, the Jaffe case turns out to be simpler than the Hernquist one; this is not unexpected, because the Jaffe gravitational potential is logarithmic, like the term appearing in the expression for f in eq. (33). In practice, f has only one minimum, for all values of the galaxy parameters. For this reason we begin the discussion with the Jaffe model.

4.1. The Jaffe model

The gravitational potential of the Jaffe (1983) density distribution is given by

$$\phi_g = \frac{GM_g}{r_g} \ln \left(\frac{r}{r + r_g} \right), \quad (37)$$

where the scale-length r_g is related to the galaxy effective radius R_e as $r_g \simeq R_e/0.7447$. From eq. (37), f in eq. (33) becomes:

$$f = \frac{\chi}{x} - \frac{\mathcal{R}}{\xi} \ln \left(\frac{x}{x + \xi} \right) + 2 \ln x. \quad (38)$$

In three cases the determination of x_{\min} and f_{\min} is trivial. First, when $\xi \rightarrow \infty$ (or $\mathcal{R} \rightarrow 0$), the galaxy contribution vanishes, and the results in Sect. 3.1 are recovered. Second, although ϕ_g is not continuous at the origin, by fixing $r > 0$ and considering the limit $r_g \rightarrow 0$, the resulting potential is that of a MBH of mass M_g ; thus, this limiting case

reduces to the problem of accretion on a MBH of total (effective) mass $(\chi + \mathcal{R})M_{\text{BH}}$, and can be treated as in Sect. 3.1. In particular, the position of the only minimum of f (i.e., of the sonic radius), and the critical value λ_t , are given by:

$$x_{\min} = \frac{\chi + \mathcal{R}}{2}, \quad \lambda_t = (\chi + \mathcal{R})^2 \lambda_{\text{cr}}, \quad (39)$$

where λ_{cr} is the critical value for the corresponding classical Bondi problem (Sect. 2). Third, for $\chi = 0$ the discussion in Appendix B shows that isothermal accretion in Jaffe potential is possible only for $\mathcal{R} \geq 2\xi$; this condition is equivalent to the requirement that $GM_{\text{g}} \geq 2r_{\text{g}}c_{\infty}^2$. We derive for x_{\min} and λ_t the expressions:

$$x_{\min} = \frac{\mathcal{R} - 2\xi}{2}, \quad \lambda_t = \frac{\mathcal{R}^2}{4\sqrt{e}} \left(1 - \frac{2\xi}{\mathcal{R}}\right)^{2-\mathcal{R}/\xi}. \quad (40)$$

This is equivalent to have $r_{\min}/r_{\text{g}} = GM_{\text{g}}/(2c_{\infty}^2 r_{\text{g}}) - 1$; for $\mathcal{R} = 2\xi$, one has that $x_{\min} = 0$ and $\lambda_t = \xi^2/\sqrt{e}$.

The general expression for x_{\min} , for assigned χ , \mathcal{R} , and ξ , is given in eq. (B2); from this expression, f_{\min} can be easily evaluated. In Appendix B we also show that there is only one minimum at $x \geq 0$. Figure 2 shows the trend of x_{\min} and λ_t with ξ , for representative values of \mathcal{R} , and $\chi = 1$. For the ease of inspection of the figure, we recall that the choice of $\mathcal{R} = 1000$ corresponds to the standard assumption about the ratio between the stellar mass and the MBH mass in spheroids (e.g. Magorrian et al. 1998); a value of $\xi \approx 100$ is representative of the case of hot gas accretion at the center of elliptical galaxies, when r_{g} is a few kpc, and r_{B} is of the order of a few tens of pc (e.g. Pellegrini 2010; see also Sect. 6). Figure 2 shows that x_{\min} for accretion in the Jaffe potential is much larger than in the classic Bondi solution ($x_{\min} = 1/2$); for reasonable $\xi \approx 100$ and $\mathcal{R} \approx 10^3$ (see above), x_{\min} reaches values of a few hundreds. This significant increase is explained by the compactness of the mass distribution that is typical of the Jaffe model. The critical λ_t is also much larger than in the classical Bondi accretion (Sect. 2). In the limiting case of $\xi \rightarrow 0$, the sonic radius x_{\min} becomes very large in a way predicted by eq. (39); this same equation also explains the trend for $\lambda_t \sim \mathcal{R}^2$ shown at low ξ in the right panel of Fig. 2. At large ξ , instead, the effect of the gravitational field of the galaxy diminishes, and correspondingly x_{\min} decreases, towards the limiting case of classical Bondi accretion; the same is true for λ_t , that tends to λ_{cr} . Finally, cases with $\chi < 1$ are not shown in Fig. 2, since their differences with the plotted curves are very small, and would be appreciated only for very large values of ξ (or small values of \mathcal{R}), i.e. if the gravitational field at the sonic radius is dominated by the presence of the MBH (see eq. 33).

The critical isothermal solution is given by

$$\mathcal{M}^2 = - \begin{cases} W \left[0, -\frac{e^{2f_{\min} - \frac{2\chi}{x}}}{e^{x^4}} \left(\frac{x}{x+\xi} \right)^{\frac{2\mathcal{R}}{\xi}} \right], & x \geq x_{\min}, \\ W \left[-1, -\frac{e^{2f_{\min} - \frac{2\chi}{x}}}{e^{x^4}} \left(\frac{x}{x+\xi} \right)^{\frac{2\mathcal{R}}{\xi}} \right], & 0 < x \leq x_{\min}. \end{cases} \quad (41)$$

An illustrative solution for the above $\mathcal{M}(x)$ is given in Fig. 1 (middle panel), for the typical values of $\mathcal{R} = 1000$ and $\xi = 100$, and for $\chi = 1$. The choice of $\chi = 1$ means no effect from the radiation pressure, thus Fig. 1 (as Fig. 2 just discussed) shows purely gravitational effects due to the galactic + MBH potentials; however, as is the case for x_{\min} and λ_t in Fig. 2, the differences in the trend of \mathcal{M} for $\chi < 1$ from those shown in Fig. 1 would be noticed only for very large ξ , or very small \mathcal{R} .

4.2. The Hernquist model

The gravitational potential of the Hernquist model is:

$$\phi_{\text{g}} = -\frac{GM_{\text{g}}}{r + r_{\text{g}}}, \quad (42)$$

where $r_{\text{g}} \simeq R_{\text{e}}/1.82$; thus, from eq. (33) one has

$$f = \frac{\chi}{x} + \frac{\mathcal{R}}{x + \xi} + 2 \ln x. \quad (43)$$

As for the Jaffe model, from the expression above one sees that in three cases the determination of x_{\min} and f_{\min} is trivial. First, when $\xi \rightarrow \infty$ (or $\mathcal{R} \rightarrow 0$), the galaxy contribution to f vanishes, and the results of Sect. 3.1 are recovered. Second, for $r > 0$ and $r_{\text{g}} \rightarrow 0$, ϕ_{g} reduces to the potential of a MBH of mass M_{g} , and the solution of Sect.

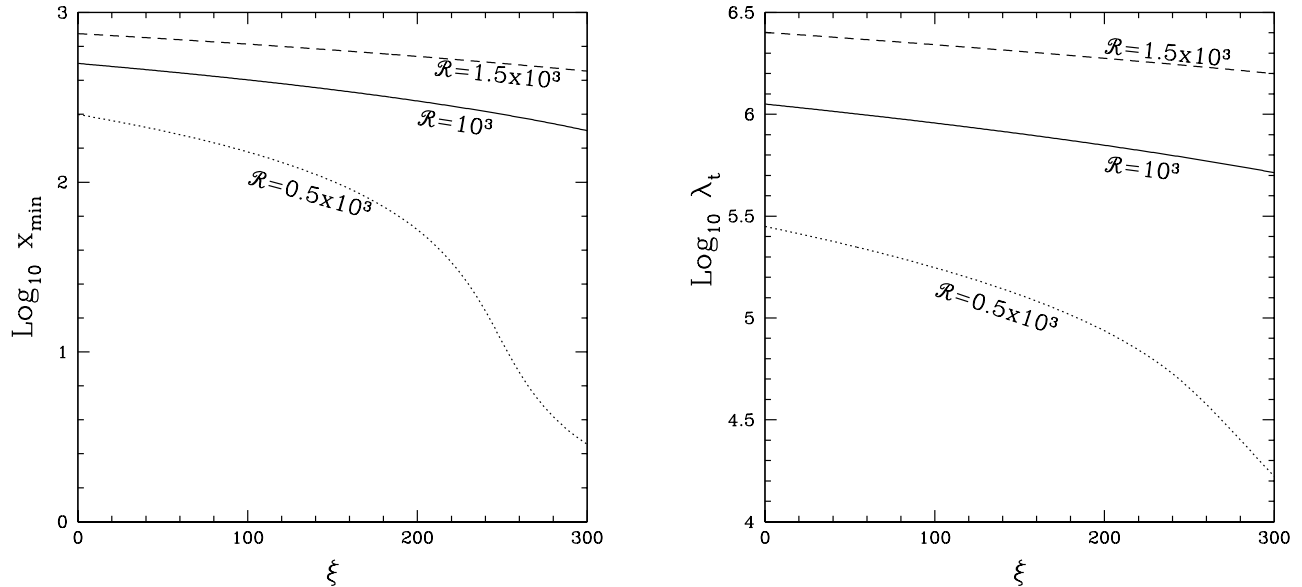


Figure 2. Left: Position of the sonic point for isothermal accretion in a Jaffe galaxy model, as a function of ξ . The curves have been determined using eq. (B2), and refer to a galaxy mass-to-MBH mass ratio of $\mathcal{R} = 500$ (dotted), 1000 (solid), 1500 (dashed); $\chi = 1$ is assumed. Right: the corresponding values of λ_t , determined following eq. (18), with $g_{\min} = 1/2$ and with f_{\min} calculated using eq. (38) for $x = x_{\min}$.

3.1 applies, for a MBH of total (effective) mass $(\chi + \mathcal{R})M_{\text{BH}}$, and eq. (39) gives the position of x_{\min} . Third, for $\xi > 0$ and $\chi = 0$, at variance with the case of the Jaffe model, no accretion is possible, because the minimum of f is attained for $x \rightarrow 0^+$, with $f_{\min} \rightarrow -\infty$, and so formally $\lambda_t = 0$ is needed. Therefore, from now on we assume $\xi > 0$ and $\chi > 0$.

The procedure to determine x_{\min} analytically, for assigned χ , \mathcal{R} , and ξ , is given in Appendix B. More than one sonic point can be present; the search for the absolute minimum x_{\min} can then be difficult. In turn, the profile $\mathcal{M}(x)$ of the critical solution can be non monotonic. Once x_{\min} is determined, one can derive f_{\min} , and then evaluate λ_t . The critical isothermal solution is then:

$$\mathcal{M}^2 = - \begin{cases} W \left(0, -\frac{e^{2f_{\min} - \frac{2\mathcal{R}}{x+\xi} - \frac{2\chi}{x}}}{e^{x^4}} \right), & x \geq x_{\min}, \\ W \left(-1, -\frac{e^{2f_{\min} - \frac{2\mathcal{R}}{x+\xi} - \frac{2\chi}{x}}}{e^{x^4}} \right), & 0 < x \leq x_{\min}. \end{cases} \quad (44)$$

Representative trends for x_{\min} and λ_t are plotted in Fig. 3, as a function of ξ , for three values of \mathcal{R} , and for $\chi = 1$. The parameters are the same chosen for the Jaffe model in Fig. 2, but the trends are very different; the difference is due to the fact that there can be one or three critical points for f (two minima and one maximum), as discussed in Appendix B. The curves in Fig. 3 refer to the absolute minimum. This different behavior is quite surprising, since both the Jaffe and Hernquist models belong to the class of γ -models, and are quite similar (for example, in projection they are both good approximations of the de Vaucouleurs surface brightness profile, over a large radial range). The only major difference is that the model density in the central regions goes as r^{-2} in the Jaffe case, and as r^{-1} in the Hernquist one.

The left panel shows how x_{\min} can vary largely. The easiest way to understand this trend is to refer to Fig. 6 in Appendix B, at a fixed \mathcal{R} , and moving from left to right. First we consider the black lines in Fig. 3, left panel, that populate small and large ξ values; in these cases, there is a *single* minimum for f . In fact, for given \mathcal{R} and sufficiently small or large ξ , there is a single minimum, according to Fig. 6. In particular, for very small ξ , the only minimum is placed at very large radii, in accordance with eq. (39); this explains the large values of x_{\min} in Fig. 3. Increasing ξ , the depth of the galactic potential well becomes shallower, and x_{\min} shifts towards inner radii. The transition from

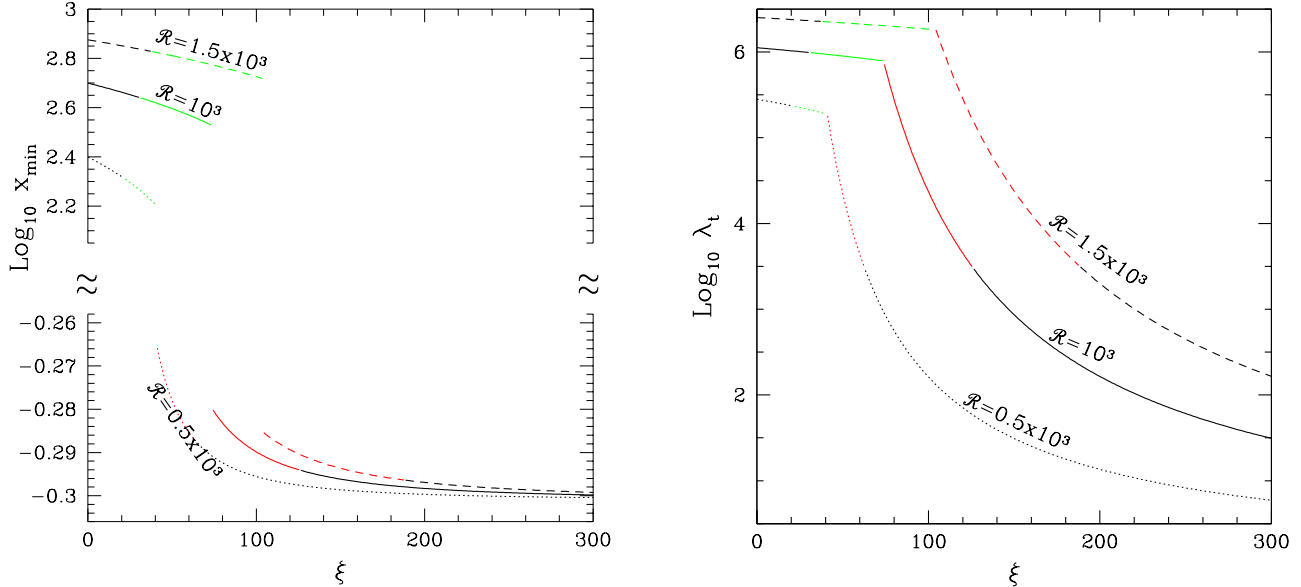


Figure 3. Left: position of the sonic point for isothermal accretion in a Hernquist galaxy model, as a function of ξ , for $\chi = 1$. The curves refer to a galaxy mass-to-MBH mass ratio of $\mathcal{R} = 500$ (dotted), 1000 (solid), 1500 (dashed). The values of x_{\min} have been determined using the procedure in Appendix B. The black lines (at low and large values of ξ) correspond to the single minimum (see Fig. 6 in Appendix B, at fixed \mathcal{R}); the green and red lines show x_{\min} when there are two minima, and respectively correspond to the solution labeled with $k = 1$ and $k = 0$ in Appendix B. The jump from the green to the red solution takes place at the value of ξ such that the two minima of f have the same value (dotted line in Fig. 6 in Appendix B); for a further increase of ξ , x_{\min} switches into the inner region. See Sect. 4.2 for more details. Right: the corresponding values of λ_t ; note how λ_t is a continuous function of ξ .

black to green lines corresponds to the appearance of the three critical points; the ξ, \mathcal{R} values are placed within the triangular region in Fig. 6, where there are two minima for f . The additional, new minimum of f appears close to the center, but the absolute minimum is still at larger radii, even if x_{\min} is decreasing; thus, the green curves show a decreasing trend with ξ , and correspond to the positions of x_{\min} given by eq. (B13), for $k = 0$. As ξ increases further, the external, absolute minimum keeps moving towards the center, while the value of f corresponding to the inner critical point [$k = 1$ in eq. (B13)], keeps decreasing. When the ξ, \mathcal{R} values hit the dotted line in Fig. 6, the values of f at the two minima become equal, and then the accretion flow develops two sonic points. One point is very close to the MBH, the other is at much larger radii. As ξ increases further, the absolute minimum becomes the point nearer to the MBH, and x_{\min} jumps from the green to the red curve. Further increasing ξ , the solution moves out of the triangular region in Fig. 6, the absolute minimum of f remains the inner one, until the minimum becomes again only one (and the x_{\min} is given again by the black curves). The behavior just described for x_{\min} also explains the reason why x_{\min} is so small (similar to that of classical Bondi accretion) in Fig. 1, left panel: the values of $\mathcal{R} = 10^3$ and $\xi = 100$ in Fig. 1 correspond to the red solid curve in Fig. 3, i.e. to the regime of very low values for x_{\min} .

The colors of the curves in the right panel reflect the fact that $\ln \lambda_t = f(x_{\min}) - 1/2$, and are thus explained by the behavior of x_{\min} described above. The curves for λ_t are continuous, and do not show jumps, because $f(x_{\min})$ decreases continuously for increasing ξ . For any fixed ξ , at fixed \mathcal{R} , λ_t increases as \mathcal{R} increases, i.e., as the galaxy mass increases.

As for the Jaffe model, cases with $\chi < 1$ would have very small differences from the curves in Fig. 3, and could be distinguished only for very large ξ or small \mathcal{R} , i.e., when the gravity of the MBH dominates.

5. AN APPLICATION: EVALUATION OF THE MASS ACCRETION RATE

As an application of the previous results, we investigate here the use of the classical Bondi solution in the interpretation of observational results, in numerical investigations, or in cosmological simulations involving galaxies and accretion on their central MBHs (see Sect. 1). In many such studies, when the instrumental resolution is limited, or the numerical resolution is inadequate, an estimate of the mass accretion rate is derived using the classical Bondi solution, taking values of temperature and density measured at some finite distance from the MBH. This procedure clearly produces an estimate that can depart from the true value, even when assuming that accretion fulfills the hypotheses of the Bondi model (stationarity, spherical symmetry, etc.). KCP16 developed the analytical set up of the

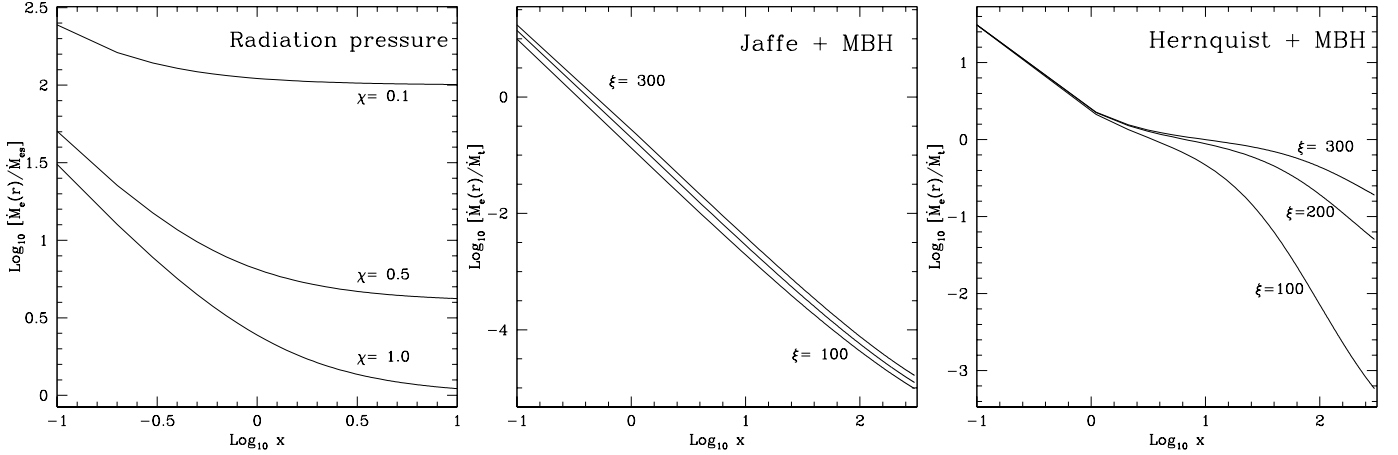


Figure 4. Ratio between the estimate of the accretion rate \dot{M}_e and the true accretion rate (\dot{M}_B , or \dot{M}_{es} , or \dot{M}_t), as a function of x (see Sect. 5). Left: classical Bondi model with the addition of the effect of electron scattering, for the three indicated values of χ ; $\chi = 1$ corresponds to classical Bondi accretion. Middle and right: accretion in Jaffe and Hernquist galaxies, with $\chi = 1$, $\mathcal{R} = 10^3$, and for three values of ξ .

problem for generic polytropic accretion, from classical Bondi accretion to the inclusion of the additional effects of radiation pressure and of an Hernquist galactic potential; they also investigated numerically the size of the deviation for some representative cases. Here we reconsider the problem, for the isothermal case that was not discussed in detail in KCP16, exploiting our analytical solution, and extending the investigation also to the case of the Jaffe potential.

We briefly start with the case of critical accretion in the classical Bondi problem. For assigned values of ρ_∞ , T_∞ , γ and M_{BH} , the Bondi radius and accretion rate are given by eqs. (6) and (8):

$$r_B = \frac{GM_{BH}}{c_\infty^2}, \quad \dot{M}_B = 4\pi r_B^2 \lambda_{cr} \rho_\infty c_\infty. \quad (45)$$

If one inserts in eq. (45) the values of $\rho(r)$ and $T(r)$ at a finite distance r from the MBH, taken along the classical Bondi solution (Sect. 2.1), and considers them as “proxies” for ρ_∞ and T_∞ , then an *estimated* value of the accretion radius (r_e) and mass accretion rate (\dot{M}_e) is obtained:

$$r_e(r) \equiv \frac{GM_{BH}}{c_s^2(r)}, \quad \dot{M}_e(r) \equiv 4\pi r_e^2(r) \lambda_{cr} \rho(r) c_s(r). \quad (46)$$

For theoretical investigations and observational works it is of obvious interest to know how much these r_e and \dot{M}_e depart from the true values r_B and \dot{M}_B , as a function of r , under the assumption that the Bondi solution holds at all radii.

For $\gamma = 1$, the isothermal case of present interest, the sound speed is constant, with $c_s(r) = c_\infty$, and then $r_e(r) = r_B$, independently of the distance from the center at which the temperature is evaluated. Also, $\dot{M}_e(r) = 4\pi r_B^2 \lambda_{cr} \rho(r) c_\infty$; at infinity, the estimate coincides² with the true value: $\dot{M}_e = \dot{M}_B$. At finite radii, from eqs. (45) and (46) the deviation of $\dot{M}_e(r)$ from \dot{M}_B can be quantified as:

$$\frac{\dot{M}_e(r)}{\dot{M}_B} = \tilde{\rho}(x) = \frac{\lambda_{cr}}{x^2 \mathcal{M}(x)}, \quad (47)$$

where the last identity derives from eq. (20), and $\mathcal{M}(x)$ is given in eq. (19). The deviation then is just given by $\tilde{\rho}(x)$ at the radius r where the “measure” is taken.

Figure 4 shows the trend of \dot{M}_e/\dot{M}_B with x (left panel, for $\chi = 1$). One sees that the use of $\rho(r)$ instead of ρ_∞ leads to an overestimate of the true accretion rate \dot{M}_B at all r ; however, the overestimate of \dot{M}_B becomes significant only for $r < r_B$.

We next apply the procedure above to the Bondi problem with radiation pressure (Sect. 3.1). Again $r_e(r) = r_B$, for $\gamma = 1$. We then quantify the difference between the true [$\dot{M}_{es} = 4\pi r_B^2 \lambda_{es} \rho_\infty c_\infty$, eq. (27)] and estimated [$\dot{M}_e(r)$ in eq.

² Note how, instead, in the monoatomic adiabatic case ($\gamma = 5/3$), one has that $\dot{M}_e(r) = \dot{M}_B$ independently of the distance from the center, i.e., $\dot{M}_e(r)$ does not deviate from the true accretion rate, while $r_e(r)$ departs from r_B (KCP16).

(46)] accretion rate, with $\rho(r)$ now evaluated along the Bondi solution including the effect of electron scattering. In this case:

$$\frac{\dot{M}_e(r)}{\dot{M}_{\text{es}}} = \frac{\lambda_{\text{cr}}\tilde{\rho}(x)}{\lambda_{\text{es}}} = \frac{\lambda_{\text{cr}}}{x^2\mathcal{M}(x)}, \quad (48)$$

where eq. (29) has been used, and $\mathcal{M}(x)$ is given by eq. (28). Thus now the deviation depends not only on the radius r where the density is taken, but also on the value of \dot{M}_{es} itself, through the parameter χ , that is included in $\mathcal{M}(x)$ [see eq. (28)]. The trend of $\dot{M}_e/\dot{M}_{\text{es}}$ as a function of x is shown in Fig. 4, left panel, for two non-special values of χ . \dot{M}_e overestimates the true accretion rate at all radii, even by a large factor if $r < r_{\text{B}}$. Of course, the overestimate increases for decreasing χ , i.e., for increasing radiation pressure. The size of the overestimate at large radii is given by eq. (48) and eq. (26), that provide $\dot{M}_e(r) = \tilde{\rho}(x)\dot{M}_{\text{es}}/\chi^2$, from which $\dot{M}_e/\dot{M}_{\text{es}} \rightarrow 1/\chi^2$ for $r \rightarrow \infty$. The behavior of $\dot{M}_e/\dot{M}_{\text{es}}$ at small radii is discussed below.

Finally, we evaluate the departure of $\dot{M}_e(r)$ in eq. (46) from the true mass accretion rate *in presence of a galaxy*, given by $\dot{M}_t = 4\pi r_{\text{B}}^2 \lambda_t \rho_{\infty} c_{\infty}$ [eq. (34)]. Taking now $\rho(r)$ along the solution for accretion within the potential of the galaxy and with electron scattering, one has:

$$\frac{\dot{M}_e(r)}{\dot{M}_t} = \frac{\lambda_{\text{cr}}\tilde{\rho}(x)}{\lambda_t} = \frac{\lambda_{\text{cr}}}{x^2\mathcal{M}(x)}. \quad (49)$$

Figure 4 shows the radial dependence of \dot{M}_e/\dot{M}_t for the Jaffe and Hernquist galaxy models. Both models have the same $\mathcal{R} = 10^3$ and the same three values of ξ ; all differences in the trend of their \dot{M}_e/\dot{M}_t are then entirely due to the different mass density profiles of these two models. The middle and right panels show a clearly different behavior from that of the left panel (no galaxy): $\dot{M}_e(r)$ provides again an overestimate for r taken in the central regions, while $\dot{M}_e(r)$ becomes a significant *underestimate* for large r . The position of the radius marking the transition from the region in which there is an overestimate, to that where there is an underestimate, depends on the specific galaxy model, and on the choice of the galaxy parameter values. An important consequence is that, for example, in numerical simulations not resolving r_{B} , \dot{M}_e should be boosted by a large factor to approximate the true accretion rate \dot{M}_t . Note how by increasing ξ the effect of the Hernquist galaxy becomes more and more similar to that of a single, very large mass concentration, and consequently \dot{M}_e becomes less and less an underestimate, at large radii. For the Jaffe model this effect is very weak for the parameters of Fig. 4.

It is instructive to find the reason for the common trend of \dot{M}_e to overestimate the true accretion rate, near the center, in all three panels of Fig. 4. This can be achieved from the expansion for $x \rightarrow 0^+$ of eq. (33), or of the supersonic branch of $W(-1, z)$ in eq. (35). In both ways, for the galaxy models chosen here, and for $\chi > 0$, one has that $\mathcal{M}(x) \sim \sqrt{2\chi}x^{-1/2}$, and so:

$$\frac{\dot{M}_e(r)}{\dot{M}_t} \sim \frac{\lambda_{\text{cr}}}{\sqrt{2\chi}x^{3/2}}, \quad x \rightarrow 0^+. \quad (50)$$

This demonstrates that the effect of the galaxy on the ratio \dot{M}_e/\dot{M}_t disappears for $x \rightarrow 0^+$; and the trend becomes that of the effect of radiation pressure, with the respective value of χ . In particular, in Fig. 4 all curves in the central region become similar to the curve for $\chi = 1$ in the left panel (that corresponds to the effect from the pure MBH). Within the range of x values of Fig. 4 the convergence to the classic ($\chi = 1$) Bondi solution has not been reached yet by the Jaffe galaxy, while instead it has been reached by the Hernquist one. This corresponds to the fact that in the central region the galaxy potential is much more important in the Jaffe model than in the Hernquist one. Such a difference in the galactic potential is also reflected in the different location of the sonic point x_{min} in the two galaxy models: x_{min} is very small for the Hernquist galaxy (see Fig. 3, for the ξ values of Fig. 4), and it is much larger for the Jaffe galaxy (Fig. 2).

For completeness we mention also the case $\chi = 0$. While isothermal stationary accretion is impossible in the Hernquist potential (Sect. 4.2), for the Jaffe model one has $\mathcal{M}(x) \sim 2\sqrt{(1 - \mathcal{R}/2\xi)\ln(x/x_{\text{min}})}$, for $x \rightarrow 0$ (provided that $\mathcal{R} \geq 2\xi$). From this expression for \mathcal{M} one obtains the analogous of eq. (50).

The expansion of $\mathcal{M}(x)$ for $x \rightarrow \infty$ explains the trend of \dot{M}_e at large distances from the MBH. It gives $\mathcal{M}(x) \sim \lambda_t e^{-(\chi+\mathcal{R})/x}/x^2$, and then:

$$\frac{\dot{M}_e(r)}{\dot{M}_t} \sim \frac{\lambda_{\text{cr}}}{\lambda_t}, \quad x \rightarrow \infty. \quad (51)$$

In the case of a galactic potential, λ_t becomes very large, and \dot{M}_e/\dot{M}_t correspondingly becomes very small, as shown in the middle and right panels of Fig. 4. In particular, λ_t is much larger, and less dependent on ξ , for the Jaffe

than for the Hernquist model (as shown by Figs. 2 and 3). This, together with eq. (51), explains why in Fig. 4 the underestimate provided by \dot{M}_e is much larger for the Jaffe than for the Hernquist galaxy; and why it is hardly dependent on ξ , in the Jaffe case, while it is largely varying with ξ , in the Hernquist one.

6. SUMMARY AND CONCLUSIONS

The classical Bondi accretion theory represents the tool commonly adopted in many investigations requiring an estimate of critical quantities as the accretion radius and the mass accretion rate; as examples, we quote here cosmological simulations, when numerical resolution is not high enough to probe in a self-consistent way the region near the central MBH, and the interpretation of observational results, when the instrumental resolution does not allow to reach the MBH surroundings. In this work we focus on the case of isothermal accretion in galaxies with central MBHs, and with radiation pressure contributed by electron scattering in the optically thin regime. All the hypotheses of classical Bondi accretion (stationarity, absence of rotation, spherical symmetry) were maintained. We show that, notably, the radial profile of the Mach number can be obtained by using the Lambert-Euler W -function (commonly implemented in computer algebra systems). Even more remarkably, for the Jaffe and Hernquist galaxies, also the value of the critical accretion parameter can be analytically calculated. As an application, we examine the problem of the bias induced on the estimates of the mass accretion rate by the adoption of the classical Bondi solution for accretion on a MBH, and of the gas density and temperature at some finite distance from the center as proxies for their values at infinity. The main results of this work can be summarized as follows.

1) For isothermal accretion towards the center of a generic spherically symmetric potential, and for a given accretion parameter, the Mach number profile can be written in terms of the W -function. The dependence of the critical accretion parameter from the properties of the Jaffe and Hernquist galaxy models with a central MBH is given analytically, even in presence of radiation pressure.

2) For the Jaffe potential, the determination of the critical accretion parameter involves the solution of a quadratic equation, and there is only one sonic point for any choice of the parameters describing the galaxy. Moreover, accretion is possible even in absence of the central MBH (for a subset of values of the galaxy parameters).

3) For the Hernquist galaxy model, the critical accretion parameter is given by the solution of a cubic equation, that is fully investigated; one or two sonic points can be present. It is also shown that isothermal accretion is not possible in a Hernquist galaxy without a central MBH.

4) The structure of the accretion flow is sensitive to the mass density profile of the host galaxy; surprisingly, it turned out to be quite different even for the two chosen galaxy models, belonging to the class of γ -models, at fixed total mass and scale-length. In fact, in a Jaffe galaxy the position of the sonic point depends smoothly on the galaxy properties; on the contrary, in the Hernquist potential the flow structure is more complex, and the position of the sonic point can jump from very large to very small distances from the center, even for a smooth variation of the galaxy parameters. For example, for the same (plausible) values of the galaxy parameters, the position of the sonic point is $\approx 400 r_B$ for the Jaffe model, and just $\approx r_B$ for the Hernquist one.

5) The size of the departure, from the true value, of estimates of the accretion rate $\dot{M}_e(r)$ based on the classical Bondi solution, and the gas properties at a finite distance r from the center, is given as a function of this distance. The departure is proportional to the local density of the accreting material. We derive the formulae for the deviation of $\dot{M}_e(r)$ for the three cases of classical Bondi accretion, of accretion with electron scattering, and of accretion on a MBH at the center of a galaxy with electron scattering (when the true rate is respectively \dot{M}_B , \dot{M}_{es} , and \dot{M}_t).

6) $\dot{M}_e(r)$ is an overestimate of \dot{M}_B , whatever the radius at which the density is taken. $\dot{M}_e(r)$ is always an even larger overestimate of \dot{M}_{es} , when radiation pressure is present; of course, the overestimate becomes larger for increasing radiation pressure. In presence of a galaxy, $\dot{M}_e(r)$ overestimates \dot{M}_t , if the density is taken in the central region, and *underestimates* \dot{M}_t if it is taken outside a few Bondi radii. The size of the overestimate, approaching the center, becomes less and less dependent on the galaxy profile, and close to that of the classical Bondi problem; the size of the underestimate, instead, is very sensitive to the details of the galaxy profile. A quantitative explanation for these two trends is given. The position of the transition between the two kinds of departure depends on the details of the density profile of the galaxy. In conclusion, caution should be exerted when proposing general recipes for the mass supply rate to the MBH.

Finally, we note that the present investigation can be expanded in an interesting respect, considering the link between the gas temperature and the galaxy properties. In fact, in the present study we kept c_∞ as a free parameter, while, in a galaxy, the gas temperature is likely linked to the depth of the potential well (i.e., it should be close to the virial temperature of the system). This means that r_B should depend on r_g and M_g , which introduces a physical scale in the problem. Remarkably, the link between the temperature and the potential can be expressed analytically for the

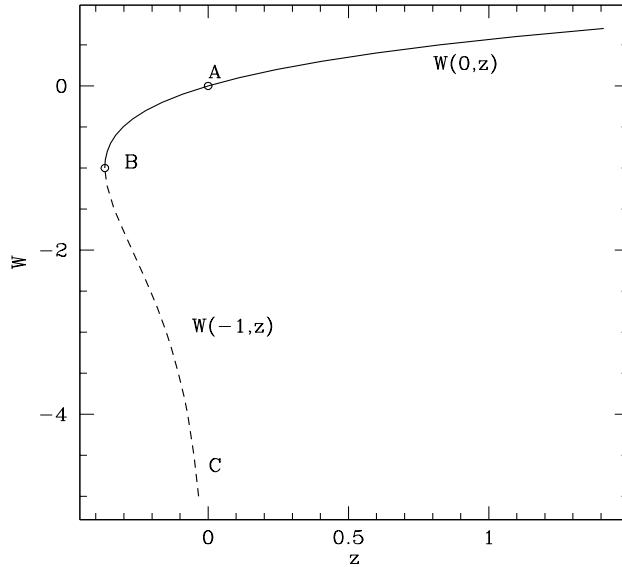


Figure A1. The real determination of the W -function. The two branches involved in the solution of the accretion problem are that of $W(0, z)$ (solid line) between the points $A = (0, 0)$ and $B = (-1/e, -1)$, and of $W(-1, z)$ (dashed line) between the points B and the asymptotic point $C = (0, -\infty)$.

two-component (stars + dark matter) Jaffe models with a central MBH (Ciotti & Ziaee Lorzad, in preparation); this will be the subject of a forthcoming work.

APPENDIX

A. A. THE LAMBERT-EULER W FUNCTION

The Lambert-Euler function $W(z)$ is a multivalued complex function implicitly defined by

$$W \exp(W) = z, \quad (\text{A1})$$

where in general z is a complex variable. As well known, several transcendental equations can be recast and solved in terms of W . For example, it can be shown that the equation

$$a X^b + c + d \ln X = Y, \quad (\text{A2})$$

for the non negative unknown X , and where a, b, c, d , and Y are quantities independent of X , has the solution

$$X^b = \frac{d}{ab} W \left[\frac{ab}{d} \exp \frac{(Y - c)b}{d} \right]. \quad (\text{A3})$$

The real determination of W is shown in Fig. 5, and it is made of two branches, called $W(0, z)$ and $W(-1, z)$. For a general discussion of the properties of the W -function we refer to the classical papers (e.g., Corless et al. 1996).

The result above shows that eq. (19) gives the required solution to the problem in Section 2, as detailed in Sect. 2.1.

B. B. THE CRITICAL PARAMETER FOR ISOTHERMAL ACCRETION IN JAFFE AND HERNQUIST MODELS WITH CENTRAL BH

From the discussion in Sect. 2 it follows that the critical value of the isothermal accretion parameter in the generalized Bondi theory is given by eq. (15). Therefore, λ_{cr} can be computed explicitly when f_{min} is: in turn, this reduces to the determination of x_{min} , i.e. the position of the *absolute* minimum of f for $x \geq 0$. In presence of a generic galaxy potential this is not possible analytically, but in KCP16 it was shown that, quite remarkably, this can be done for the Hernquist model with a central BH in the general polytropic case with electron scattering, by solving a cubic equation.

For simplicity the explicit solution was not given, although all the needed information to determine the number and position of the critical points of f were reported and discussed. Here we give the explicit solution for the Jaffe and Hernquist galaxy models in the isothermal case and electron scattering.

B.1. The Jaffe model

At variance with the Hernquist model, where x_{\min} (and so f_{\min} and λ_t) can be computed analytically for $1 \leq \gamma \leq 5/3$ (KCP16), in the Jaffe case the explicit expression of x_{\min} can be obtained only in the isothermal case, $\gamma = 1$. In this case, however, the situation is much simpler than for the Hernquist model. In fact, independently of the value of the galaxy parameters, there is only a single minimum, as can be proved by a study of eq. (37):

$$f' = \frac{2g(x)}{x^2(\xi + x)}, \quad g = x^2 - \frac{\mathcal{R} + \chi - 2\xi}{2}x - \frac{\chi\xi}{2}. \quad (\text{B4})$$

The discriminant of the function g is non-negative for all physical (i.e., positive) values of \mathcal{R} , ξ and χ , so that f' has two real solutions. Moreover, the Descartes' sign rule shows that for $\xi > 0$ and $\chi > 0$ one solution of $g = 0$ is negative and one is positive, corresponding to the searched position of the minimum of f ,

$$x_{\min} = \frac{\mathcal{R} + \chi - 2\xi + \sqrt{(\mathcal{R} + \chi - 2\xi)^2 + 8\chi\xi}}{4}. \quad (\text{B5})$$

In the peculiar case of $\chi = 0$ (i.e., when radiation pressure cancels exactly the gravitational field of the BH, and the effective potential is only due to the galaxy), a solution of the accretion problem is possible only for $\mathcal{R} \geq 2\xi$, with x_{\min} and λ_t given in Sect. 4.1. When $\mathcal{R} \leq 2\xi$, the function g in eq. (B1) is positive for $x > 0$, so that the minimum is attained at the origin. When $\mathcal{R} = 2\xi$, we have $x_{\min} = 0$ (the sonic point is at the origin), $f_{\min} = 2 \ln \xi$, so that it is *finite*, and $\lambda_t = \xi^2/\sqrt{e}$, consistently with the limit of λ_t for $\mathcal{R} \rightarrow 2\xi$ in eq. (42). For $\mathcal{R} < 2\xi$, $f_{\min} = -\infty$, and so no accretion is possible, because one would derive $\lambda_t = 0$. These different behaviors for the Jaffe model with $\chi = 0$ arise because the galaxy potential is logarithmic, with the possibility to “compensate” near the origin (at least for some choices of \mathcal{R} and ξ) the term $2 \ln x$, even in absence of the gravitational field of the MBH. As we will see, the more “regular” nature of the Hernquist potential at the center makes this impossible, and no accretion can take place in the isothermal case for $\chi = 0$, independently of the galaxy parameters.

B.2. The Hernquist model

In case of isothermal accretion in a Hernquist galaxy with central BH and radiation pressure due to electron scattering, the critical points of f are placed at the non-negative zeroes of

$$f' = \frac{2g(x)}{x^2(\xi + x)^2}, \quad g = x^3 - \frac{\mathcal{R} + \chi - 4\xi}{2}x^2 + \xi(\xi - \chi)x - \frac{\xi^2\chi}{2}. \quad (\text{B6})$$

The limiting cases of $\xi = 0$ and $\chi = 0$ are discussed in Sect. 4.2; here we discuss the more realistic case of $\xi > 0$ and $\chi > 0$. The constant term for g in eq. (B3) is strictly negative, while the coefficient of the cubic term is positive; thus, f has always at least one minimum for $x > 0$. However, g can have three real zeros, for some particular values of \mathcal{R} , ξ and χ . It is therefore important to have quantitative criteria to determine the number and position of the critical points of f , and in particular of the absolute minimum f_{\min} that is required.

The existence and the position of the zeros of g for assigned values of the parameters can be determined from the theory of cubic equations, as follows. With the substitution

$$x = z + \frac{\mathcal{R} + \chi - 4\xi}{6}, \quad (\text{B7})$$

the function $g(x)$ in eq. (B3) reduces to the canonical depressed form $g_c(z) = z^3 + pz + q$, with

$$p = -\frac{\mathcal{R}^2 - 2\mathcal{R}(4\xi - \chi) + (2\xi + \chi)^2}{12}, \quad q = -\frac{\mathcal{R}^3 - 3\mathcal{R}^2(4\xi - \chi) + 3\mathcal{R}(10\xi^2 - 2\xi\chi + \chi^2) + (2\xi + \chi)^3}{108}, \quad (\text{B8})$$

so that once the zeroes z_k ($k = 0, 1, 2$) of $g_c(z)$ are known, the corresponding solutions x_k of $g(x)$ are obtained from eq. (B4). As well known the number of real zeros of a cubic equation with real coefficients is determined by the sign of the function

$$R \equiv \frac{q^2}{4} + \frac{p^3}{27} = \frac{\xi^2\mathcal{R} [\chi\mathcal{R}^2 - (\xi^2 + 10\chi\xi - 2\chi^2)\mathcal{R} + (2\xi + \chi)^3]}{432}, \quad (\text{B9})$$

where the last expression is obtained from eq. (B5). This expression can also be obtained from the more general eq. (C4) in KCP16, evaluated for $\gamma = 1$.

All the roots appearing in the following equations must be intended as arithmetic roots. When $R > 0$ there is only one real solution given by

$$z_0 = \sqrt[3]{\sqrt{R} - q/2} - \frac{p/3}{\sqrt[3]{\sqrt{R} - q/2}}, \quad (\text{B10})$$

and so z_0 determines the location of the only minimum of f , i.e. $x_{\min} = x_0$. By inspection of eq. (B6), it follows that $R > 0$ both for small and large values of \mathcal{R} at fixed ξ , and for small and large values of ξ at fixed \mathcal{R} . The exact boundary of the region in the (ξ, \mathcal{R}) plane corresponding to $R > 0$ can be determined rigorously. In fact, for $\xi < 4\chi$ the discriminant of the quadratic function of \mathcal{R} in eq. (B6) is negative, and so $R > 0$ independently of the value of \mathcal{R} . For $\xi \geq 4\chi$, in accordance with Descartes' sign rule, there are two positive values of \mathcal{R} :

$$\mathcal{R}_{\min, \max} = \frac{\xi^2 + 10\chi\xi - 2\chi^2 \pm \sqrt{\xi(\xi - 4\chi)^3}}{2\chi}, \quad (\text{B11})$$

so that $R < 0$ for $\mathcal{R}_{\min} < R < \mathcal{R}_{\max}$, and $R > 0$ outside this range. Therefore, all points outside the open triangular region in Fig. 6 correspond to models with a single minimum for f , given by eqs. (B4) and (B7). Note that for $\xi \rightarrow \infty$, $\mathcal{R}_{\min} \sim 8\xi$ and $\mathcal{R}_{\max} \sim \xi^2/\chi$.

Along the two critical curves defined by eq. (B8) in Fig. 6, $R = 0$ and $g_c(z)$ has a single real root, and a double (and so also real) root, given respectively by:

$$z_0 = \frac{3q}{p}, \quad z_{1,2} = -\frac{z_0}{2}. \quad (\text{B12})$$

The positions of the associated zeros of $g(x)$ are given by a surprisingly simple expression. In fact, along the lower solid curve in Fig. 6, when $\mathcal{R} = \mathcal{R}_{\min}$, one has that:

$$0 < x_0 = \frac{\xi \left[\xi - 2\chi - \sqrt{\xi(\xi - 4\chi)} \right]}{4\chi} \leq x_{1,2} = \frac{\xi + \sqrt{\xi(\xi - 4\chi)}}{2}, \quad (\text{B13})$$

while for $\mathcal{R} = \mathcal{R}_{\max}$ (the upper solid curve in Fig. 6) one has that:

$$0 < x_{1,2} = \frac{\xi - \sqrt{\xi(\xi - 4\chi)}}{2} \leq x_0 = \frac{\xi \left[\xi - 2\chi + \sqrt{\xi(\xi - 4\chi)} \right]}{4\chi}. \quad (\text{B14})$$

In both cases, being $x_{1,2}$ a double root, f has an *inflection* point there, and the only minimum is placed at $x_{\min} = x_0$ given in eqs. (B10)-(B11).

When $\xi = 4\chi$ (and so $\mathcal{R} = 27\chi$) all solutions collapse (heavy dot in Fig. 6), and there is only a third-order minimum, placed at

$$x_{\min} = x_0 = x_1 = x_2 = 2\chi, \quad f_{\min} = 5 + 2 \ln(2\chi) \quad (\text{B15})$$

where the last identity follows from eq. (45). Note how $f_{\min} \rightarrow -\infty$ and $\lambda_{\text{cr}} \rightarrow 0$ for $\chi \rightarrow 0$.

For $R < 0$ [when necessarily $p < 0$ from eq. (B6)], i.e. for $\mathcal{R}_{\min} < \mathcal{R} < \mathcal{R}_{\max}$, there are three real roots of $g_c(z)$, given by:

$$z_k = 2\sqrt{-\frac{p}{3}} \cos\left(\frac{\varphi}{3} + \frac{2\pi k}{3}\right), \quad k = 0, 1, 2 \quad (\text{B16})$$

with:

$$0 \leq \varphi \equiv \arccos\left(-\frac{q}{2}\sqrt{-\frac{27}{p^3}}\right) \leq \pi. \quad (\text{B17})$$

It is simple to prove that $z_1 < z_2 < z_0$; moreover Descartes' sign rule applied to eq. (B3) with $\mathcal{R}_{\min} < \mathcal{R} < \mathcal{R}_{\max}$ shows that the three real zeros are positive, so that, from eq. (B4), x_1 , x_2 , and x_0 correspond to a minimum, a maximum, and a minimum of f , respectively. In the case $R < 0$ we must then determine what is the position of the absolute minimum among x_1 and x_0 . This is illustrated by the following procedure.

Suppose we fix a value of $\xi > 4\chi$ and we start increasing \mathcal{R} from a very small value, i.e., we move vertically in the plane of Fig. 6. Initially there is only one minimum $x_{\min} = x_0$ given by eq. (B7), so that f increases monotonically for $x > x_0$. When \mathcal{R} reaches the lower curve $R = 0$ ($\mathcal{R} = \mathcal{R}_{\min}$), a double root $x_{1,2}$ appears, corresponding to an inflexion point of f , while $x_{\min} = x_0$, as in eq. (B10). For $\mathcal{R}_{\min} < \mathcal{R} < \mathcal{R}_{\max}$, now $R < 0$, the double root splits, and eq. (B13) applies. The absolute minimum corresponds to z_1 , while z_2 and z_0 correspond to a maximum and a minimum of f ,

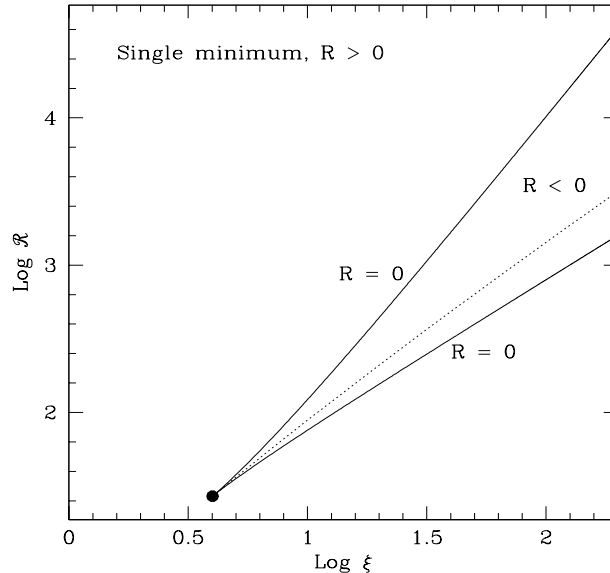


Figure B2. Sign of R in eq. (B6) across the (\mathcal{R}, ξ) plane, for Hernquist galaxies, in the illustrative case $\chi = 1$. The two solid lines correspond to eq. (B8), and start at $(\xi, \mathcal{R}) = (4\chi, 27\chi)$. For ξ and \mathcal{R} within the triangular region defined by the two solid lines there are two minima and one maximum for f in eq. (45). Along the dotted line there are two sonic points for the accretion flow, since the two minima of f have the same depth.

respectively. Increasing further \mathcal{R} , z_2 moves towards z_1 , while the minimum corresponding to z_0 deepens; when the dotted curve is reached, the two minima of f have the same value, i.e. $f(x_1) = f(x_0)$, and the accretion flow has two sonic points. Above the dotted curve the absolute minimum jumps at z_0 , and the minimum at z_1 becomes less and less pronounced. When $\mathcal{R} = \mathcal{R}_{\max}$ the two zeroes z_1 and z_2 merge, so that $x_{1,2}$ becomes the new inflection point of f , while the absolute minimum is now at x_0 , again given by eq. (B7). For higher values of \mathcal{R} , there is only one minimum given by eq. (B7).

REFERENCES

- Baganoff, F.K., et al. 2003, ApJ 591, 891
Bondi, H., 1952, MNRAS 112, 195
Bu, D.-F., Yuan, F., Wu, M., Cuadra, J. 2013, MNRAS 434, 1692
Cao, X. 2016, ApJ 833, 30
Chandrasekhar, S., 1939, *An introduction to the study of stellar structure*, The University of Chicago press
Choi, E., Ostriker, J.P.O., Naab, T., et al. 2016, MNRAS in press (arXiv:1610.09389)
Ciotti, L. and Ostriker, J. P., 2012, AGN Feedback in Elliptical Galaxies: Numerical Simulations, in *Hot Interstellar Matter in Elliptical Galaxies*, Astrophysics and Space Science Library, vol. 378, p.83, eds. D.-W. Kim, S. Pellegrini
Cranmer, S.R. 2004, Am. J. Phys. 72, 11
DeGraf, C., Dekel, A., Gabor, J., Bournaud, F. 2017, MNRAS 466, 1462
Dehnen, W., 1993, MNRAS 265, 250
Di Matteo, T., Colberg, J., Springel, V., Hernquist, L., Sijacki, D. 2008, ApJ 676, 33
Fukue, J., 2001, PASJ 53, 687
Frank, J., King, A. and Raine, D., 1992, *Accretion power in astrophysics.*, Camb. Astrophys. Ser., Vol. 21, Cambridge University Press
Herbst, R.S. 2015, PhD Thesis, University of Witwatersrand
Hernquist, L., 1990, ApJ 356, 359
Hopkins, P., Hernquist, L., Cox, T.J., et al. 2006, ApJS 163, 1
Hopkins, P., Hernquist, L., Cox, T.J., et al. 2007, ApJ 669, 45
Jaffe, W., 1983, MNRAS 202, 995
Kormendy, J., Richstone, D. 1995, ARA&A 33, 581
Kormendy, J., Ho, L.C. 2013, ARAA 51, 511
Korol, V., Ciotti, L., Pellegrini, S. 2016, MNRAS 460, 1188 (KCP16)
Lusso, E., and Ciotti, L., 2011, A&A 525, 115
Magorrian, J., Tremaine, S., Richstone, D., et al. 1998, AJ 115, 2285
Park, K., Ricotti, M. 2011, ApJ 739, 2
Park, K., Ricotti, M., Natarajan, P., Bogdanovic, T., Wise, J.H. 2016, ApJ 818, 184
Park, K.-H., Wise, J.H., Bogdanović, T. 2017, in press on ApJ (arXiv:1704.0786)
Pellegrini, S. 2005, ApJ 624, 155
Pellegrini, S. 2010, ApJ 717, 640
Rafferty, D. A., McNamara, B. R., Nulsen, P. E. J., & Wise, M. W. 2006, ApJ 652, 216
Russell, H. R., Fabian, A. C., McNamara, B., Broderick, A. E., 2015, MNRAS 451, 588
Sijacki, D., Springel, V., Di Matteo, T., Hernquist, L. 2007, MNRAS 380, 877

Tremaine, S., Richstone, D. O., Byun, Y.-I., et al. 1994, AJ 107,
634
Volonteri, M., Capelo, P.R., Netzer, N., et al. 2015, MNRAS 449,
1470

Wong, Ka-Wah, Irwin, J.A., Shcherbakov, R. V., Yukita, M.,
Million, E. T., Bregman, J. N. 2014, ApJ 780, 9
Yuan, F., Narayan, R. 2014, ARAA 52, 529